Physics in Medicine & Biology



PAPER

# Mixed-size spot scanning with a compact large momentum acceptance superconducting (LMA-SC) gantry beamline for proton therapy

To cite this article: Wei Wang *et al* 2024 *Phys. Med. Biol.* **69** 115011

IOP Publishing Phys. Med. Biol. 69 (2024) 115011 https://doi.org/10.1088/1361-6560/ad45a6

Physics in Medicine & Biology

IPEM Institute of Physics and Engineering in Medicine

RECEIVED
20 February 2024

REVISED
13 April 2024

ACCEPTED FOR PUBLICATION
30 April 2024

PUBLISHED
20 May 2024

PAPER

# Mixed-size spot scanning with a compact large momentum acceptance superconducting (LMA-SC) gantry beamline for proton therapy

**Wei Wang**[1], **Xu Liu**[1], **Yicheng Liao**[1], **Yiling Zeng**[2], **Yu Chen**[1], **Benzhaoxia Yu**[1], **Zhiyong Yang**[3], **Hao Gao**[4] and **Bin Qin**[1]

[1] State Key Laboratory of Advanced Electromagnetic Technology, School of Electrical and Electronic Engineering, Huazhong University of Science and Technology, Wuhan 430074, People's Republic of China
[2] Department of Medical Physics, School of Physics and Technology, Wuhan University, Wuhan 430072, People's Republic of China
[3] Cancer Center, Union Hospital, Tongji Medical College, Huazhong University of Science and Technology, Wuhan 430022, People's Republic of China
[4] Department of Radiation Oncology, University of Kansas Medical Center, United States of America

**E-mail:** lxhustliu@hust.edu.cn

**Keywords:** proton therapy, compact beamline design, mixed-size spot scanning, delivery efficiency

## Abstract

*Objective*. Lowering treatment costs and improving treatment quality are two primary goals for next-generation proton therapy (PT) facilities. This work will design a compact large momentum acceptance superconducting (LMA-SC) gantry beamline to reduce the footprint and expense of the PT facilities, with a novel mixed-size spot scanning method to improve the sparing of organs at risk (OAR). *Approach*. For the LMA-SC gantry beamline, the movable energy slit is placed in the middle of the last achromatic bending section, and the beam momentum spread of delivered spots can be easily changed during the treatment. Simultaneously, changing the collimator size can provide spots with various lateral spot sizes. Based on the provided large-size and small-size spot models, the treatment planning with mixed spot scanning is optimized: the interior of the target is irradiated with large-size spots (to cover the uniform-dose interior efficiently), while the peripheral of the target is irradiated with small-size spots (to shape the sharp dose falloff at the peripheral accurately). *Main results*. The treatment plan with mixed-size spot scanning was evaluated and compared with small and large-size spot scanning for thirteen clinical prostate cases. The mixed-size spot plan had superior target dose homogeneities, better protection of OAR, and better plan robustness than the large-size spot plan. Compared to the small-size spot plan, the mixed-size spot plan had comparable plan quality, better plan robustness, and reduced plan delivery time from 65.9 to 40.0 s. *Significance*. The compact LMA-SC gantry beamline is proposed with mixed-size spot scanning, with demonstrated footprint reduction and improved plan quality compared to the conventional spot scanning method.

## 1. Introduction

More than 50% of cancer patients receive radiation therapy. Proton therapy (PT) is regarded as the treatment of choice for children, adolescents, and young adult patients facing complex, large, and reoccurring tumors, owing to its reduced integral dose and negligible exit dose to normal tissues (Mohan and Grosshans 2017, Paganetti 2018). Despite the number of proton facilities increasing rapidly worldwide, the demand far exceeds the availability for proton treatment (Yan *et al* 2023), for which a low-cost and compact PT facility is needed (Schippers 2016, Bortfeld and Loeffler 2017).

Currently, cyclotron-based PT facilities account for two-thirds of the total installations. The accelerator and gantry are the two largest, heaviest, and most expensive components for cyclotron-based PT facilities. Much work has gone into developing lighter and smaller cyclotrons using superconducting magnets

(Radovinsky *et al* 2014, Godeke *et al* 2020, Ebara *et al* 2023). However, reducing the footprint of the beamline to fit inside a traditional treatment room is incredibly difficult as the gantries have dimensions of 10–12 m in diameter and 100–200 tons in weight. Some studies have studied the large momentum acceptance superconducting (LMA-SC) gantry beamline, which uses superconducting magnets to reduce the size and allows for a lighter and simpler mechanical structure, reducing total weight by a maximum factor of 8–10 (Wan *et al* 2015, Gerbershagen *et al* 2016a, Nesteruk *et al* 2019, Zhao *et al* 2021). In cyclotron-based PT facilities, energy modulation is completed in the degrader system before the gantry. Due to scattering and nuclear interactions during energy degradation (Gerbershagen *et al* 2016b), a set of collimators and the energy slit are needed to limit the beam size, divergence, and energy spread. However, those components will contribute to the total footprint of the PT system.

Nesteruk *et a* proposed mounting the degrader and the beam size collimator on the LMA-SC gantry beamline, thus further reducing the size of the whole system dramatically (Nesteruk *et al* 2019). These designs of the LMA-SC gantry beamline have removed the energy slit because the beams with a large momentum spread can be transported to the isocenter. This avoids the extra beam loss at the energy slit and allows fewer stacked energy layers to cover the tumors, thus improving the delivery efficiency (Wang *et al* 2023). Unfortunately, the larger distal dose-off is negative for improving the sparing of organs at risk (OAR). Additionally, the lateral spot profile of the spots with large momentum spread would be distorted at the large scanning position due to the dispersion effect of the scanning magnets (Gerbershagen *et al* 2016a). If the spot shape of each position isn't modeled precisely in the treatment planning system, the dose difference between the delivered and planned spot doses will occur, especially for spots far from the isocenter. To resolve the issue, an ideal scenario (Yan *et al* 2017, Kraan *et al* 2018) that uses small-size spots at the periphery of targets and large-size spots at the inside of targets is helpful. Also, the flexibility of selecting spot sizes for other cases or situations is desirable (Mohan *et al* 2017) since the proton spot size increases with depth, influencing the normal tissue complication probabilities resulting from PT. Therefore, an efficient method for compact PT equipment that dynamically adjusts the spot size at the isocenter is needed.

In the present study, we propose a compact LMA-SC gantry beamline that integrates the degrader system and energy slit into the gantry. This scheme allows delivering the spots with different lateral and longitudinal sizes by changing the collimator size and moving the energy slit. Then, the mixed-size spot scanning method, which uses larger lateral and longitudinal size spots on the inside of the target and smaller spots on the peripheral of the target, was used to improve the dose quality.

## 2. Method

### 2.1. The design of the compact LMA-SC gantry beamline

As shown in figure 1(a), the compact beamline consists of the fixed-field beamline, the ultra-fast degrader system, the achromatic bending, and the nozzle section. For the proposed compact LMA-SC gantry beamline, the beam shaping components such as the degrader, beam size collimator, and energy slit are moved from the fixed-field beamline to the gantry, and the last two bend magnets use the alternating-gradient canted-cosine-theta (AG-CCT) SC magnets. Before the degrader, the fixed-field beamline transports the highest energy beam ($E = 235$ MeV, $dp/p = \pm 0.1\%$), and thereby, the magnetic field remains constant during treatment. The proton energy is modulated by varying the stopping length of the degrader material but at the expense of increased transverse emittance and beam energy spread.

The AG-CCT achromatic bending section is fully symmetric since the symmetric layout considerably suppresses higher-order aberrations. The beamline was designed with the large momentum acceptance (LMA) property to avoid magnetic field changes of the AG-CCT. As shown in figures 1(b) and (c), with the unchanged magnetic field, $-10\% \sim +10\%$ momentum deviation proton beams can be delivered to the isocenter. This technology can achieve fast bi-directional energy change in the degrader system without re-tuning the entire beamline magnets during treatments. By employing the commercially available linear motors suited for precise longitudinal motions, the degrader system could achieve ultra-fast energy changes within 50 ms per step.

### 2.2. The delivery of spots with different sizes

The collimator set (Col #1 and Col #2) and energy slit are employed to control the beam quality due to the increase of transverse emittance and beam momentum spread after the energy degrader. Instead of using static collimators, the lateral spot size at the isocenter can be varied by changing the collimator size. Due to the LMA properties, the spots with a larger momentum spread can be delivered to the isocenter. However, larger longitudinal spot sizes impede improving the distal dose-off. Therefore, besides the variable collimator size, the movable energy slit is placed in the middle of the achromatic bending section, which gives the option of using the large or standard momentum spread beam during the treatment.

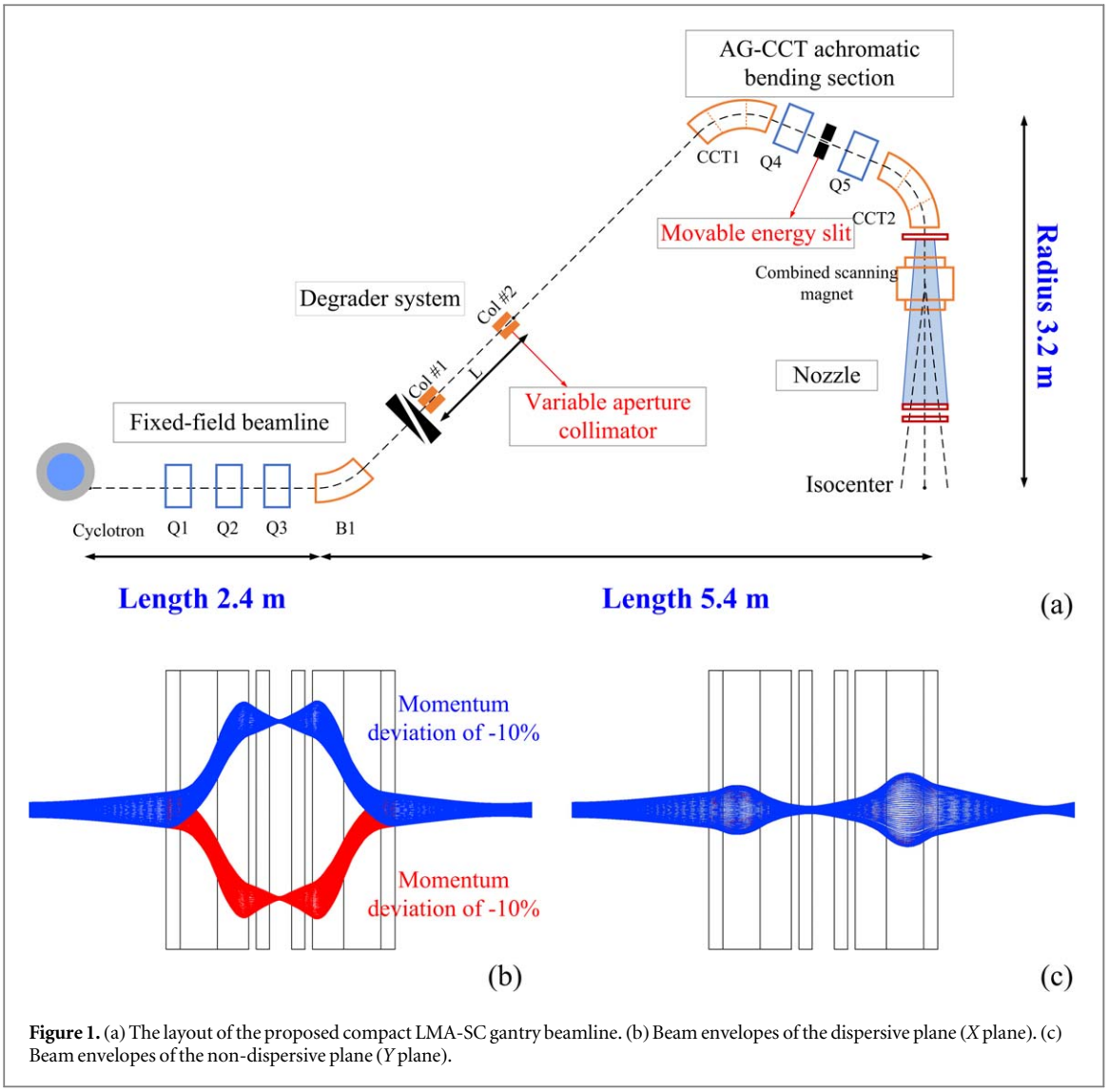


**Figure 1.** (a) The layout of the proposed compact LMA-SC gantry beamline. (b) Beam envelopes of the dispersive plane (*X* plane). (c) Beam envelopes of the non-dispersive plane (*Y* plane).

**Table 1.** The beam parameters and beamline setting of the large-size spot mode and small-size spot mode.

| | | Small-size spot | Large-size spot |
|---|---|---|---|
| Beamline setting | Col #2 size | 5.3 mm | 10.6 mm |
| | Energy slit gap | 5 mm | N/A (removed) |
| Spot parameters | Designed lateral size | 2.5 mm | 5 mm |
| | Transverse emittance | 5 pi*mm*mrad | 10 pi*mm*mrad |
| | Momentum spread | ±0.1% ~ ±0.5% | ±0.1% ~ ±2.71% |

Two pencil beam spot models with different spot sizes and the corresponding beamline settings have been demonstrated in table 1. By adjusting the Col# 2 size, the spots with different lateral sizes (2.5 and 5 mm) are provided. Besides the variable lateral spot size, the beam momentum spread can also be controlled by adjusting the gap of the energy slit. After the energy slit is removed, the spots with natural momentum spread (±0.1% ~ ±2.71%) are delivered to the isocenter.

### 2.3. Beam library

*2.3.1. Generation of the compact LMA-SC gantry beamline beam library*

After the beamline optics and beamline component settings are determined, the beam phase space data at the isocenter should be modeled for the subsequent generation of the TPS basic data. Because of different physics interactions, the start-to-end beamline simulation was used to simulate the beam data, which adopts separate

**Table 2.** The start-to-end separate modeling method for generating the LMA-SC gantry beamline beam library.

| | Physics interactions | Simulation software | Statistical evaluations |
|---|---|---|---|
| Fixed-field beamline | Transportation | COSY INFINITY | Beam phase space |
| Degrader system | Transportation | | Nominal energy |
| | Stopping | TOPAS | Beam phase space |
| | Scatter | | |
| | Nuclear interaction | | Transmission $t_1$ |
| First half AG-CCT bending | Transportation | COSY INFINITY | Beam phase space |
| Movable energy slit | Transportation | | |
| | Stopping | TOPAS | Beam phase space; |
| | Scatter | | Transmission $t_2$ |
| | Nuclear interaction | | |
| Second half AG-CCT bending | Transportation | COSY INFINITY | Beam phase space |
| Nozzle | Transportation | | Nominal energy |
| | Stopping | TOPAS | Beam phase space |
| | Scatter | | |
| | Nuclear interaction | | Transmission $t_3$ |

modeling from the exit of the cyclotron to the isocenter. The beamline simulation method was depicted in table 2. More proton interactions in matter exist during the beam delivery. Therefore, besides COSY INFINITY (Makino and Berz 2006), TOPAS (Perl *et al* 2012) was used to calculate phase space variations and beam loss. Using the methods, the LMA-SC gantry beamline beam library of proton beam energies, energy spectrum, and lateral widths at the isocenter was determined. Also, the beam intensity at the isocenter was inferred

$$I_1 = t_1 t_2 t_3 I_0, \tag{1}$$

where the $I_0$ is the extracted cyclotron beam current, and the $t_1$, $t_2$, and $t_3$ are the beam transmission efficiency of the degrader system, energy slit, and nozzle section.

*2.3.2. Generation of the TPS basic beam data*

To begin, the partial dose generated by a single proton spot with energy $E_{\text{beam}}$ centered at $(x_0, y_0)$ can be described as

$$D(E_{\text{spot}}, x, y, z) = c_1 ddd(E_{\text{spot}}, z) \frac{N}{2\pi\sigma_1(z)\sigma_2(z)} e^{-\left(\frac{(x_0-x)^2}{2\sigma_1(z)} + \frac{(y_0-y)^2}{2\sigma_2(z)}\right)}, \tag{2}$$

where the $c_1$ is the converting factor, the $ddd(E_{\text{spot}}, z)$ is the depth-dose distributions ($ddd$) as a function of penetration depth $z$ for the given initial beam energy $E_{\text{spot}}$. $N$ is the total number of protons, and $\sigma(z)$ is the lateral width ($1\sigma$) with the depth $z$.

Therefore, to facilitate the dose calculation for TPS requirements, the $ddd$, lateral spot size, and range ($R_{80}$) in the water were calculated in advance for each nominal energy. To obtain these basic beam data, the Monte-Carlo software TOPAS was used to calculate the three-dimensional dose distribution in water. The initial beam phase space parameters were automatically set by looking up the LMA-SC beamline beam library. The binning resolution was adjusted to 0.1 mm in depth and 0.5 mm laterally, and the total simulated number of 2000 000 primaries for trading off the accuracy and efficiency. Then, we integrated the 3D dose distribution in water laterally to obtain the $ddd$ curve of each nominal energy beam. Also, the spot size $\sigma(E, z)$ was inferred by fitting the lateral dose profile as a single Gaussian function. Instead of importing the spot size $\sigma(E, z)$, the scatter spot size $\sigma_1(E, z)$ data with the depth $z$ was imported

$$\sigma_1(z) = \sqrt{\sigma^2(z) - \sigma_0^2}, \tag{3}$$

where the $\sigma(E, z)$ is the spot size at the different depths, and the $\sigma_0$ is the spot size in air.

After that, the large and small-size spot models, including the spot size, scatter spot size, range, and ddd curves, were created and imported into the matRad for treatment planning studies.

### 2.4. Mixed-size spot scanning method

Based on the hybrid spot placement (Meier *et al* 2017, ur Rehman *et al* 2022), we proposed a mixed-size spot scanning method in which the small-size spot is placed onto the outermost of the target using the target contour as a guide, and the large-size spot is placed onto the inside of the target using the rectilinear grid, as shown in figure 2. For mixed-size spot placement, the original spot set $\Omega(X, Y, E)$ was created with finer lateral spacing (3 mm) and larger longitudinal spacing (equal to the Bragg peak width of the large-size spot). The spot energy

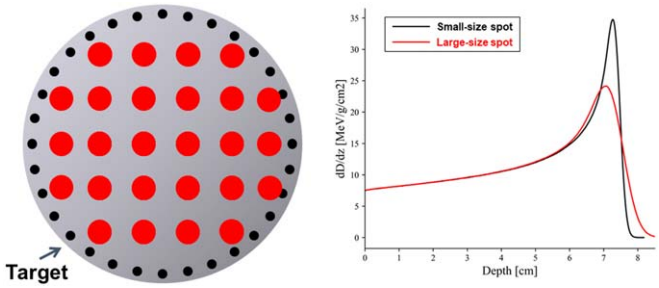


**Figure 2.** The illustration of the mixed-size spot scanning methods.

**Table 3.** Dose constraints for prostate cases.

| Structure | Type | Constraints |
|---|---|---|
| PTV | $D_{2\%}$ | <77 * 1.07 Gy |
| | $D_{98\%}$ | >77 * 0.95 Gy |
| | HI | <10% |
| Rectum | $V_{50}$ | <40% |
| | $V_{70}$ | <20% |
| Bladder | $V_{40}$ | <35% |
| femoral head | $V_{40}$ | <5% |

was determined by matching the water-equivalent path length to the $R_{80}$ of the large-size spot. Firstly, spots positioned in the two outermost contours of each layer, and located in the last layer were picked out and then formed the small size spot $\Omega_S(X, Y, E)$. The remaining spots were sparse with the coarse lateral spacing (6 mm) and defined as the large-size spot set $\Omega_L(X, Y, E)$. Because of the larger lateral spot size and longitudinal spot size, the lateral spot spacing and longitudinal energy layer spacing can be increased, resulting in fewer energy layers and spots. The small-size spots at the target's peripheral improve the sparing of OAR and avoid the dose discrepancy due to the beam shape distortion at the large scanning angle. For each energy layer, the large-size spots are first delivered, and then the beamline setting is switched to deliver the small-size spot.

The mixed-size spot treatment plan (using large and small-size spots) was designed and compared with the large and small-size spot treatment plans to investigate the potential of the mixed-size beam scanning delivery method. Because of the different spot sizes laterally and longitudinally, the lateral spot spacing (3 mm and 6 mm for small and large-size spot plans, respectively) and longitudinal spacing (equal to the Bragg peak width $d80$—$p80$ of each energy layer) were chosen differently. The comparative study used data from thirteen prostate cancer patients, and every patient was included in a retrospective study approved by the institutional review board. The treatment plans used multifield optimization with two fields (90° and 270°) and were designed using the open-source MATLAB-based treatment planning software matRad (Wieser *et al* 2017 and Liao *et al* 2024) The treatment plan used a constant relative biological effectiveness (RBE) conversion factor of 1.1 and a prescription dose of 77 GyRBE in 35 fractions to the PTV $D_{95\%}$. The dose constraints were established, as shown in table 3.

### 2.5. Plan evaluation

The dose quality of the treatment plans was assessed using dose–volume metrics. $D_{98\%}$ and $D_{2\%}$ were evaluation criteria for target coverage description, as recommended by the ICRU report 78 (Jones *et al* 2007). The mean dose and $D_{2\%}$ at OAR were also compared to evaluate the OAR dose. Additionally, the target homogeneity index (HI) and conformal index (CI) were calculated using the following equation

$$\mathrm{HI} = \frac{D_{2\%} - D_{98\%}}{D_{50\%}}, \tag{5}$$

$$\mathrm{CI} = \frac{V_{95\%,\mathrm{PTV}}}{V_{\mathrm{PTV}}} \times \frac{V_{95\%,\mathrm{PTV}}}{V_{95\%}}, \tag{6}$$

where $D_{2\%}$, $D_{50\%}$, and $D_{98\%}$ are the minimum dose to 2%, 50%, and 98% volume receiving at least highest dose, respectively, $V_{95\%,\mathrm{PTV}}$ is PTV volumes receiving at least 95% prescription dose, $V_{\mathrm{PTV}}$ is the total volume in the PTV, and $V_{95\%}$ is total treatment volume.

The mixed-size spot plan, the large-size spot plan, and the small-size spot plan were robustly evaluated, which was performed by simulating 28 uncertainty scenarios (14 SE scenarios × 2 RE scenarios) for each of the

plans (Korevaar *et al* 2019). The sampling of the setup error scenarios included the six principal directions ((±3 mm, 0, 0), (0, ±3 mm, 0), (0, 0, ±3 mm)) and the eight diagonals from the center to the vertices ($(\pm\sqrt{3}$ mm, $\pm\sqrt{3}$ mm, $\pm\sqrt{3}$ mm)) and the range error assuming the uncertainties of ± 3%. The plan robustness was compared and evaluated regarding the 5–95th percentile value of DVH matrices.

Statistical analysis was performed using the non-parameter Wilcoxon signed-rank test, using SPSS 26.0 software (IBM Inc., Armonk, NY, USA), and derived $p$ values of 0.05 were considered statistically significant.

Also, besides the dose quality, the number of spots and energy layers were evaluated. For the large-size spot plan and the small-size spot plan, the total delivery time per fraction consists of the energy layer switching time $T_l$, spot traveling time $T_s$, and dose delivery time per spot $T_d$. However, the beam mode change occurs when irradiating a layer for mixed-size spot scanning. The beamline changing time $T_b$ required to change the collimator size and move the energy slit should be considered in addition to the time components of the three previously mentioned. The delivery time was calculated based on the machine parameters, according to the equations (7)–(11)

$$T = \sum_{i=1}^{N_E}\left(T_{l,i} + T_{b,i} + \sum_{j=1}^{N_{s,i}}(T_{s,ij} + T_{d,ij})\right), \tag{7}$$

$$T_{l,i} = 50\ \text{ms}, \tag{8}$$

$$T_{b,i} = \begin{cases} 0\ \text{ms} & \text{without beam mode changing} \\ 50\ \text{ms} & \text{with beam mode changing} \end{cases}, \tag{9}$$

$$T_{s,ij} = 2\ \text{ms}, \tag{10}$$

$$T_{d,ij} = \frac{N_{p,ij}}{I_i}, \tag{11}$$

where $N_E$ is the number of the energy layer, $N_{s,i}$ is the number of spots in the $i$th energy layer, energy layer switching time $T_l$ and the beamline changing time $T_b$ is set as 50 ms per step, the spot switching time $T_s$ is set as 2 ms per spot, $N_{p,ij}$ is the prescribed charge of this spot, and $I_i$ is the beam current of the $i$th layer.

## 3. Results

### 3.1. Large and small-size spots

Even though the lateral spot size of the large and small-size spots is designed to be 2.5 and 5 mm at the isocenter, the beam position monitor, ionization chambers, and the gas in the path of the scanning nozzle influence the spot size. As shown in figure 3(a), the lateral spot size of the large spots (5.2–6.3 mm) was larger than that of the small spots (2.8–4.6 mm). The removal of the energy slit resulted in a larger longitudinal spot size and momentum spread for the large spots in the 70–160 MeV range, as shown in figures 3(b) and (c). However, in the high energy range of 160–235 MeV, the beam momentum spread and longitudinal size of the large spots were comparable to those of the small spots because of the less noticeable range straggling effect during the energy degradation. As shown in figure 3(d), due to employing the smaller collimator and removing the energy slit, the beam current of small spots is lower than that of the large spots.

### 3.2. Plan quality comparison

Figures 4(a)–(c) shows doses on an axial CT slice for a selected patient, with results from mixed-size spot plan (figure 4(a)), large-size spot plan (figure 4(b)), and small-size spot plan (figure 4(c)). The same phenomenon was observed in the plot of dose–volume histogram (figures 4(d)–(f)), i.e. the mixed-size spot plan had a reduction in the dose of OAR compared to the large-size spot plan and comparable protection to the nearby OAR compared to the small-size spot plan. Besides offering superior sparing of OAR, the mixed-size spot plan provided a more homogeneous dose than the large-size spot plan but a similar target dose quality compared to the small-size spot plan.

Also, the plan dose–volume metrics of the treatment plans were compared and evaluated. Table 4 shows the average and range of the plan dosimetric parameters of the target and OAR for the selected 13 prostate patients. Compared with the large-size spot plans, the mixed-size spot plans had the less hot spots (PTV $D_{2\%}$: 79.5 GyRBE versus 80.5 GyRBE, $p = 0.001$; CTV $D_{2\%}$: 79.4 GyRBE versus 80.4 GyRBE, $p = 0.001$), better target dose homogeneity (PTV HI: 2.8% versus 4.0%, $p = 0.001$; CTV HI: 1.85 versus 2.63%, $p = 0.001$), and better protection of OAR (Bladder $D_{\text{mean}}$: 23.6 GyRBE versus 26.7 GyRBE, $p = 0.002$; Rectum $D_{\text{mean}}$: 19.5 GyRBE versus 23.9 GyRBE, $p = 0.002$;). In comparison with the small-size spot plans, the mixed-size spot plans had comparable hot spots (PTV $D_{2\%}$: 79.5 GyRBE versus 79.5 GyRBE, $p = 0.753$; CTV D2%: 79.4 GyRBE versus 79.3 GyRBE, $p = 0.463$), comparable dose homogeneity (PTV HI: 2.8% versus 2.7%, $p = 0.173$; CTV HI: 1.85%

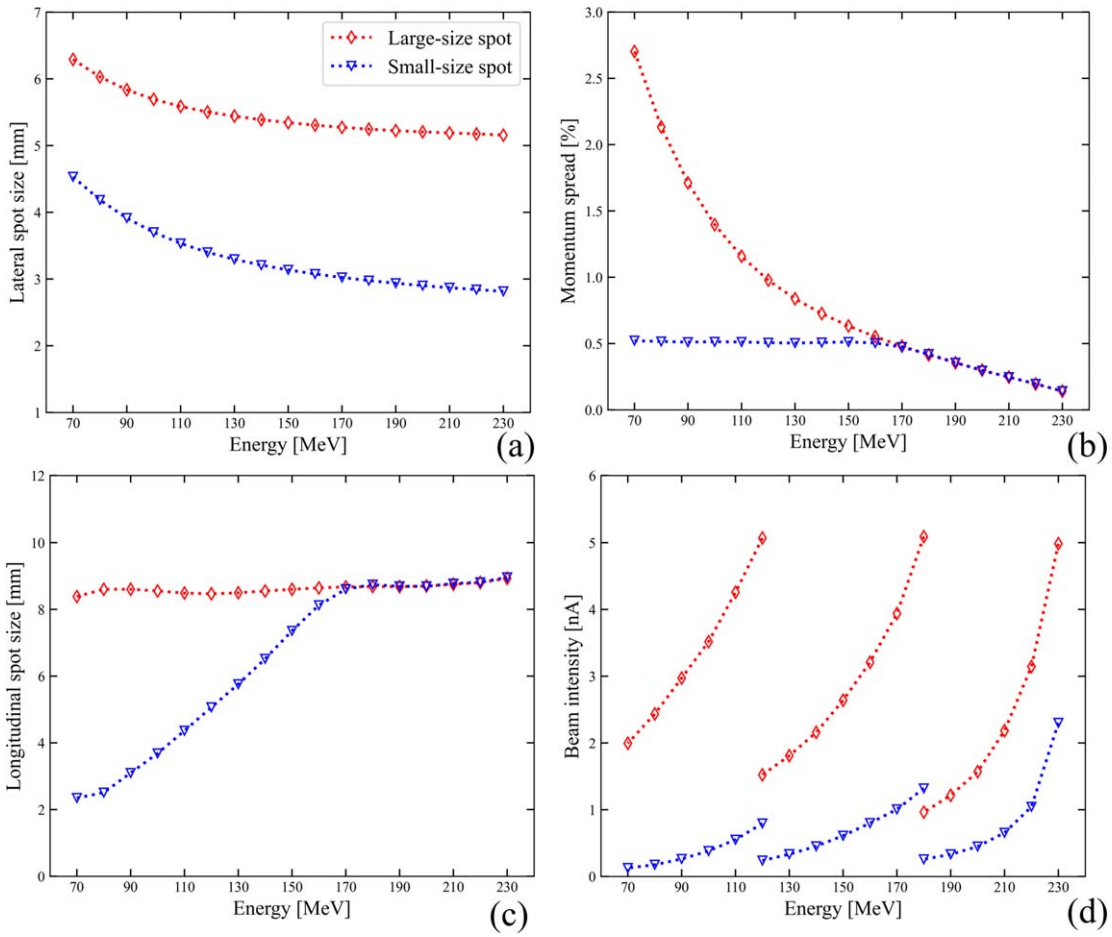


**Figure 3.** The comparison of lateral spot size (a), beam momentum spread (b), longitudinal spot size (c), and beam intensity (d) between the large-size spot and the small-size spot.

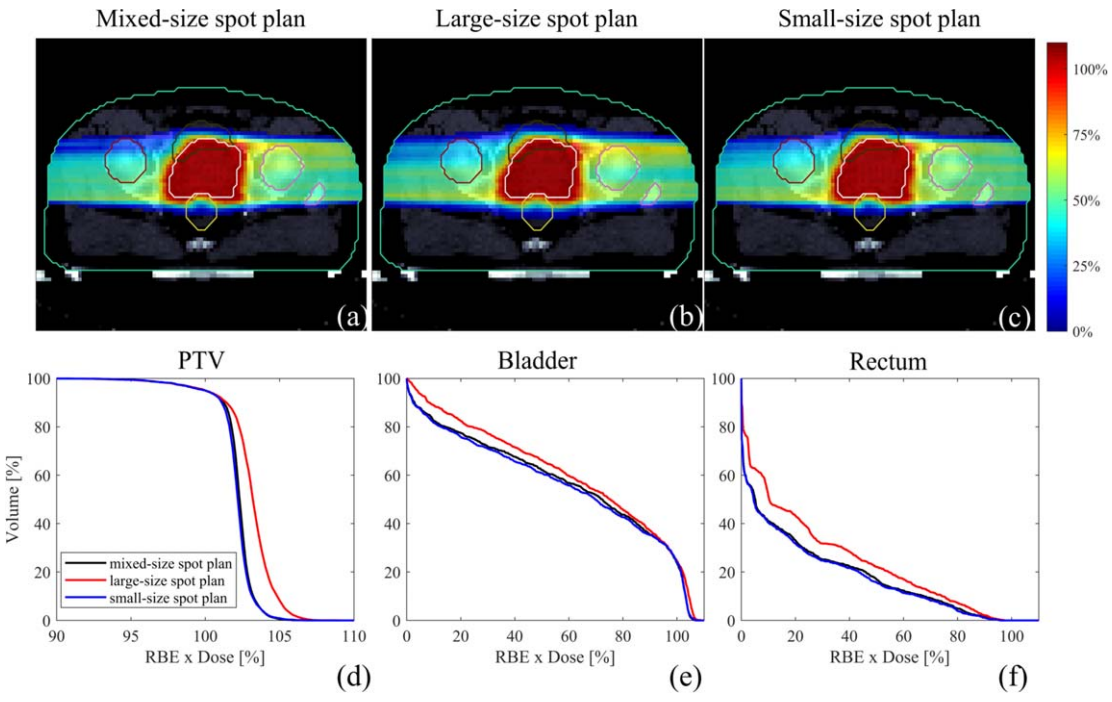


**Figure 4.** Dose distributions for mixed-size spot plan (a), large-size spot plan (b), and small-size spot plan (c) and the dose volume histograms for PTV (d), bladder (e), and rectum (f).

**Table 4.** The plan dose parameters and delivery time (average and range) for the mixed, large, and small-size spot plans of prostate cases.

| | | Mixed-size spot plan | Large-size spot plan | Small-size spot plan |
|---|---|---|---|---|
| PTV | $D_{2\%}$ (GyRBE) | 79.5 (78.8–80.9) | 80.5 (79.3–81.6)* | 79.5 (78.5–80.5) |
| | $D_{98\%}$ (GyRBE) | 76.0 (75.3–76.5) | 75.9 (75.2–76.4)* | 76.1 (75.2–76.6) |
| | CI | 0.79 (0.74–0.84) | 0.79 (0.74–0.84) | 0.80 (0.75–0.86)** |
| | HI (%) | 2.8 (1.9–4.2) | 4.0 (2.3–5.3)* | 2.7 (1.6–3.7) |
| CTV | $D_{2\%}$ (GyRBE) | 79.4 (78.9–80.3) | 80.4 (79.5–81.5)* | 79.3 (78.8–80.2) |
| | $D_{98\%}$ (GyRBE) | 77.4 (76.9–78.0) | 77.6 (76.8–78.3)* | 77.2 (76.7–77.7)** |
| | HI (%) | 1.85 (1.52–2.42) | 2.63 (1.95–3.42)* | 1.90 (1.52–2.46) |
| Bladder | $D_{mean}$ (GyRBE) | 23.6 (5.4–47.5) | 26.7 (6.6–50.5)* | 23.1 (5.3–46.7)** |
| Rectum | $D_{mean}$ (GyRBE) | 19.5 (8.7–34.1) | 23.9 (11.4–37.0)* | 19.4 (8.4–36.3) |
| Femur left | $D_{mean}$ (GyRBE) | 25.9 (15.5–42.8) | 27.7 (15.4–44.8)* | 26.9 (14.9–42.8)** |
| | D2 (GyRBE) | 44.8 (37.5–51.9) | 45.1 (40.3–52.6) | 46.1 (40.5–51.5) |
| Femur right | $D_{mean}$ (GyRBE) | 27.2 (15.9–45.9) | 29.5 (18.4–46.1)* | 28.0 (16.6–45.7) |
| | D2 (GyRBE) | 43.8 (39.9–51.7) | 43.9 (39.9–51.7) | 45.4 (39.0–51.5) |
| Total spots ($10^3$) | | 6.9 (2.3–25.5) | 3.3 (0.9–12.4) | 14.8 (4.0–62.1) |
| Total energy layers | | 29 (20–51) | 28 (20–51) | 34 (20–66) |
| Total beam change | | 24 (16–46) | 0 | 0 |
| Spot traveling time (s) | | 13.9 (4.7–51.1) | 6.5 (2.0–24.9) | 29.6 (8.1–124.2) |
| Energy layer switching time (s) | | 1.4 (0.9–2.5) | 1.3 (0.9–2.5) | 1.6 (0.9–3.2) |
| Beam mode changing time (s) | | 1.2 (0.8–2.3) | 0 | 0 |
| Dose delivery time (s) | | 24.7 (7.1–87.7) | 8.9 (2.3–32.5) | 34.7 (9.1–131.6) |
| Total beam delivery time (s) | | 40.0 (12.8–135.9) | 16.7 (5.5–57.9) | 65.9 (19.4–259.1) |

* $p < 0.05$ while comparing the mixed and large-size spot plans.
** $p < 0.05$ while comparing the mixed and small-sized spot plans.

**Table 5.** The mean (min–max) of 5–95th percentile DVH metrics of the mixed, large, and small-size spot plans of all 13 prostate patients.

| | 5–95th percentile | Mixed-size spot plan | Large-size spot plan | Small-size spot plan |
|---|---|---|---|---|
| CTV | $D_{2\%}$ (GyRBE) | 1.08 (0.54–3.71) | 1.59 (0.74–5.61)* | 1.98 (0.97–5.16)** |
| | $D_{98\%}$ (GyRBE) | 3.09 (0.67–8.45) | 3.01 (0.51–5.82) | 4.23 (1.75–8.55)** |
| | HI (%) | 1.94 (0.71–5.04) | 2.37 (1.11–5.39)* | 3.33 (1.55–6.28)** |
| Bladder | $D_{mean}$ (GyRBE) | 7.83 (2.44–14.2) | 8.15 (2.59–13.7)* | 7.95 (2.55–14.4) |
| Rectum | $D_{mean}$ (GyRBE) | 11.4 (7.08–15.4) | 11.5 (7.64–15.3) | 11.3 (7.00–15.1)** |

* $p < 0.05$ while comparing the mixed and large-size spot plans.
** $p < 0.05$ while comparing the mixed and small-sized spot plans.

versus 1.90%, $p = 0.173$), and comparable protection of the bladder and rectum (Bladder $D_{mean}$: 23.6 GyRBE versus 23.1 GyRBE, $p = 0.004$; Rectum $D_{mean}$: 19.5 GyRBE versus 19.4 GyRBE, $p = 0.075$).

Concurrently, the mean (max–min) of 5–95th percentile DVH metrics of CTV and OARs for all 13 patients was demonstrated in table 5. The mixed-size spot plans were most robust than the large-size spot plan (5–95th percentile CTV D2%: 1.08 versus 1.59, $p = 0.007$; HI: 1.94 versus 2.37, $p = 0.039$) and small-size spot plan (5–95th percentile CTV D2%: 1.08 versus 1.98, $p = 0.001$; CTV D98%: 3.09 versus 4.23, $p = 0.001$; HI: 1.94 versus 3.33, $p = 0.001$).

### 3.3. Plan delivery efficiency

Mixed-size spot scanning provides better target dose quality and sparing of OAR but at the cost of sacrificing delivery efficiency compared to large-size spot scanning. As shown in table 4, the delivery time of the mixed-size spot plans was increased from 16.7 to 40.0 s compared with the large-size spot plan and reduced from 65.9 to 40 s compared with the small-size spot plan. The large-size spot plan has larger lateral and longitudinal spacing because of its larger spot size. Thus, the number of spots in the large-size spot plan is less than those in the mixed and small-size spot plans. Therefore, the average spot starveling time of the mixed-size spot plan was more than that of the large-size spot plan (13.9 s versus 6.5 s) and less than that of the small-size spot plan (13.9 s versus 29.6 s). Similarly, the narrow Bragg peak of the small-size spot leads to more energy layers are required in the small-size spot plans. The average energy layer switching time of the mixed and large-size spot plan was less than that of the small-size spot plan (1.3 s versus 1.6 s). Besides the energy changing and spot switching, the beamline

changing also consumes the dead time for mixed-size spot scanning. As shown in figure 3(d), the beam intensity of the large-size spot is higher than the small-size spot plan. Therefore, the average dose delivery time of the mixed-size spot plan was more than that of the large-size spot plan (24.7 s versus 8.9 s) and less than that of the small-size spot plan (24.7 s versus 34.7 s).

## 4. Discussion

In this contribution, we have proposed a design of a compact LMA-SC gantry beamline in which the energy slit is placed in the middle of the achromatic bending section. In contrast to the prior design (Wan *et al* 2015, Gerbershagen *et al* 2016a, Nesteruk *et al* 2019, Zhao *et al* 2021), this system offers the choice of selecting spots with different lateral sizes and momentum spread, thus sharpening the dose fall-off and preventing the distortion of the spot shape at the large transverse scanning angles. The present analysis of this exploratory methodology study reveals that mixed-size spot scanning significantly improves the target dose quality and the sparing of OAR with better robustness compared to large-size spot scanning. This mixed-size spot scanning based on the compact LMA-SC gantry beamline has an important contribution toward implementing high-quality PT treatment and bringing down the cost of facilities.

Our results show that the proposed mixed-size spot scanning method presents superior target dose homogeneity, the sparing of OAR, and plan robustness. The additional dead time required to change the spot mode will be acceptable if the move components are equipped with high-performance linear motors. The mixed-size spot plan also demonstrated comparable target dose homogeneity, comparable protection of OAR, and better plan robustness than the small-size spot plan. It is generally believed that the small-size spot plan is less robust for set-up and range error and suffers a more severe impact from interplay effects when treating moving targets than the larger-size spot plan (Dowdell *et al* 2013, Grassberger *et al* 2013). However, when robust optimization is considered for treatment planning, the plan using the small-size spot provides better robust dose quality than the large-size spot plan as the optimizer has more freedom to meet the robust dose (Liu *et al* 2018). The mixed-size spot plans trade off the beam delivery efficiency and robustness dose quality, providing another treatment planning method for PT.

Although the mixed-size spot scanning only uses two proton spot models in this work, more spot models can be provided by adjusting the energy slit gap and collimator size for treating various tumors. It's easy to dynamically change the spots with different sizes for the proposed method. However, many particles were stopped by copper blocks, which led to beam loss. Increasing or decreasing the focusing force of the quadrupole is an effective method to deliver spots with different lateral spot sizes (Schreuder and Shamblin 2020). However, the extra quadrupole magnets will increase the footprint and weight of the gantry. The momentum cooling method is another method to adjust the beam momentum spread to avoid significant beam loss (Maradia *et al* 2023). On the other hand, due to the weak range straggling effect of the degrader in the high energy range (160–240 MeV), the large-size spot has the same longitudinal size as the small-size spot. In the future, the ridge filter can be placed in the degrader system to increase the longitudinal size of the spot with high energy (Maradia *et al* 2022).

In this paper, we have presented a new compact LMA-SC gantry beamline as a solution to deliver a mixed-size spot. Compared with the IBA Proteus® One (Pidikiti *et al* 2018) (Ion Beam Applications, Louvain-la-Neuve, Belgium; deployed in 2014) (Pidikiti *et al* 2018), the radius of the LMA-SC gantry beamline could be significantly reduced from more than 5 to 3.2 m due to adopting the AG-CCT SC magnets. The beam shape components were moved from the fixed-field beamline to the gantry, further reducing the footprint of the PT facilities from 10.5 to 7.8 m. The compact system will shrink hospital costs and make PT technology affordable. Another advantage of the compact PT equipment is that it can provide ultra-fast bi-directional energy change by employing the fast degrader system without ramping the magnets. The energy changing time can be significantly reduced from around 200 ∼800 to 50 ms. The spots with larger longitudinal and lateral sizes also allow fewer energy layer and spot changes to minimize the beam-off time. Reducing the beam delivery time enable greater hospital throughput and consequently lower treatment costs (Yap *et al* 2021). Remarkably, the ultra-fast energy change is an advantage for the highly efficient volumetric rescanning and brings the possibility of implementing tumor tracking (Fattori *et al* 2020, Actis *et al* 2023, Giovannelli *et al* 2023). Additionally, modulating the proton energy upstream of the beamline to adapt the depth of tumors could avoid the energy change within the large momentum acceptance; thus, the ultra-high dose rate radiation could be achieved (Gao *et al* 2022, Kang *et al* 2022, Wei *et al* 2022, Liu *et al* 2023).

This study has several limitations. The proposed compact beamline is still in the design stage, and the beam phase space parameters are calculated using the Monte Carlo simulation. Due to the dispersion effect of a larger momentum spread beam, the spot shape is different at different deflecting positions. We have investigated the dynamic adjustment of the quadrupole strength to ensure that the beam shape is consistent with the field size of

$25 \times 25$ cm$^2$ (XXXX), which is the same as that of the Varian ProBeam® 360° PT system (Shang *et al* 2020) (field size $25 \times 25$ cm$^2$) and larger than IBA Proteus® One (Pidikiti *et al* 2018) (field size $20 \times 24$ cm$^2$). To reduce the difference between the planned dose and the delivered dose further, the mixed-size spot scanning method uses small spots with smaller energy spread at the larger deflect position to avoid spot shape distortion, which is an alternative to model spot shape for all positions of the scanning field in the treatment planning system. However, more experimental data is needed to verify our design and method. On the other hand, removing the degrader system and the energy slit component from the fixed beamline to the gantry beamline reduces the volumes and footprints, but it brings the challenge of radiation shielding. Inevitable beam loss occurs in the degrader system section, and smaller radiation fields are generated in the energy slit section (Talanov *et al* 2017). Radiation shielding and protection will be carefully designed for future work.

Another limitation is that the conventional line-by-line scanning path (zig-zag) is unsuitable. The unique scanning method, in which the large-size spot is delivered and then switched to the small-size spot, should be integrated into the treatment plan system for mixed-size scanning. On the other hand, the calculation of treatment time should rely on log files, but we quantitatively evaluated treatment time through designed machine parameters in this study.

## 5. Conclusions

In this study, we have presented a compact LMA-SC gantry beamline design for miniaturizing PT facilities. The move energy slit is placed into the middle of the achromatic bending section, and the collimator size can be adjusted, which provides the spots with different lateral and longitudinal spot sizes. Based on the different spot models, the mixed spot scanning method is used to improve the dose penumbra and the sparing of OAR. Our compact beamline design shows considerable potential to reduce the size of PT facilities while maintaining a high treatment standard.

## Data availability statement

All data that support the findings of this study are included within the article (and any supplementary information files).

## Conflict of interest

The authors declare no conflict of interest.

## Funding

This work was supported by the National Natural Science Foundation of China (12205111, 11975107).

## ORCID iDs

Wei Wang https://orcid.org/0000-0002-0284-8414
Xu Liu https://orcid.org/0000-0002-9067-3393

## References

Actis O *et al* 2023 A bi-directional beam-line energy ramping for efficient patient treatment with scanned proton therapy *Phys. Med. Biol.* **68** 175001

Bortfeld T R and Loeffler J S 2017 Three ways to make proton therapy affordable *Nature* **549** 451–3

Dowdell S, Grassberger C, Sharp G C and Paganetti H 2013 Interplay effects in proton scanning for lung: a 4D Monte Carlo study assessing the impact of tumor and beam delivery parameters *Phys. Med. Biol.* **58** 4137–56

Ebara Y *et al* 2023 Performance of cryogen-free superconducting magnet in isochronous cyclotron for proton therapy *IEEE Trans. Appl. Supercond.* **33** 1–4

Fattori G, Zhang Y, Meer D, Weber D C, Lomax A J and Safai S 2020 The potential of Gantry beamline large momentum acceptance for real time tumour tracking in pencil beam scanning proton therapy *Sci. Rep.* **10** 15325

Gao H *et al* 2022 Simultaneous dose and dose rate optimization (SDDRO) of the FLASH effect for pencil-beam-scanning proton therapy *Med. Phys.* **49** 2014–25

Gerbershagen A, Baumgarten C, Kiselev D, van der Meer R, Risters Y and Schippers M 2016b Measurements and simulations of boron carbide as degrader material for proton therapy *Phys. Med. Biol.* **61** N337–48

Gerbershagen A, Meer D, Schippers J M and Seidel M 2016a A novel beam optics concept in a particle therapy gantry utilizing the advantages of superconducting magnets *Z. Med. Phys.* **26** 224–37
Giovannelli A C *et al* 2023 Exploring beamline momentum acceptance for tracking respiratory variability in lung cancer proton therapy: a simulation study *Phys. Med. Biol.* **68** 195013
Godeke A *et al* 2020 Research at varian on applied superconductivity for proton therapy *Supercond. Sci. Tech.* **33** 064001
Grassberger C *et al* 2013 Motion interplay as a function of patient parameters and spot size in spot scanning proton therapy for lung cancer *Int. J. Radiat. Oncol. Biol. Phys.* **86** 380–6
Jones D, Suit H D, Kanematsu N, Tatsuzaki H and Tsujii H 2007 Prescribing, recording, and reporting proton-beam therapy *ICRU Report* 78 (https://doi.org/10.1093/jicru_ndm021)
Kang M, Wei S, Choi J I, Lin H and Simone C B 2022 A universal range shifter and range compensator can enable proton pencil beam scanning single-energy bragg peak FLASH-RT treatment using current commercially available proton systems *Int. J. Radiat. Oncol. Biol. Phys.* **113** 203–13
Korevaar E W *et al* 2019 Practical robustness evaluation in radiotherapy—a photon and proton-proof alternative to PTV-based plan evaluation *Radiother. Oncol.* **141** 267–74
Kraan A C, Depauw N, Clasie B, Giunta M, Madden T and Kooy H M 2018 Effects of spot parameters in pencil beam scanning treatment planning *Med. Phys.* **45** 60–73
Liu C *et al* 2018 Impact of spot size and spacing on the quality of robustly optimized intensity modulated proton therapy plans for lung cancer *Int. J. Radiat. Oncol. Biol. Phys.* **101** 479–89
Liu R *et al* 2023 An Integrated physical optimization framework for proton stereotactic body radiation therapy FLASH treatment planning allows dose, dose rate, and linear energy transfer optimization using patient-specific ridge filters *Int. J. Radiat. Oncol.*Biol.*Phys.* **116** 949–59
Makino K and Berz M 2006 Cosy infinity version 9 *Nucl. Instrum. Methods Phys. Res.* A **558** 346–50
Maradia V *et al* 2022 Universal and dynamic ridge filter for pencil beam scanning particle therapy: a novel concept for ultra-fast treatment delivery *Phys. Med. Biol.* **67** 225005
Maradia V, Meer D, Dölling R, Weber D C, Lomax A J and Psoroulas S 2023 Demonstration of momentum cooling to enhance the potential of cancer treatment with proton therapy *Nat. Phys.* **19** 1437–44
Meier G *et al* 2017 Contour scanning for penumbra improvement in pencil beam scanned proton therapy *Phys. Med. Biol.* **62** 2398–416
Mohan R, Das I J and Ling C C 2017 Empowering intensity modulated proton therapy through physics and technology: an overview *Int. J. Radiat. Oncol. Biol. Phys.* **99** 304–16
Mohan R and Grosshans D 2017 Proton therapy—present and future *Adv. Drug Deliv. Rev.* **109** 26–44
Nesteruk K P, Calzolaio C, Meer D, Rizzoglio V, Seidel M and Schippers J M 2019 Large energy acceptance gantry for proton therapy utilizing superconducting technology *Phys. Med. Biol.* **64** 175007
Liao Y, Liu X, Wang W, Yang Z and Qin B 2024 Design study of a large momentum acceptance proton therapy gantry utilizing AG-CCT magnets *Nuclear Science and Techniques* (in press)
Paganetti H 2018 *Proton Therapy Physics* (CRC Press)
Perl J, Shin J, Schumann J, Faddegon B and Paganetti H 2012 TOPAS: an innovative proton Monte Carlo platform for research and clinical applications *Med. Phys.* **39** 6818–37
Pidikiti R *et al* 2018 Commissioning of the world's first compact pencil-beam scanning proton therapy system *J. Appl. Clin. Med. Phys.* **19** 94–105
Radovinsky A, Minervini J V, Miller C E, Bromberg L, Michael P C and Maggiore M 2014 Superconducting magnets for ultra light and magnetically shielded, compact cyclotrons for medical, scientific, and security applications *IEEE Trans. Appl. Supercond.* **24** 1–5
Schippers J M 2016 Miniaturizing proton therapy: a technical challenge with unclear clinical impact *Int. J. Radiat. Oncol. Biol. Phys.* **95** 149–53
Schreuder A N and Shamblin J 2020 Proton therapy delivery: what is needed in the next ten years? *Br. J. Radiol.* **93** 20190359
Shang C Y *et al* 2020 Beam characteristics of the first clinical 360°-rotational compact scanning pencil beam proton treatment system and comparisons against a multi-room system *Int. J. Radiat. Oncol.*Biol.*Phys.* **108** e360–1
Talanov V *et al* 2017 Neutron doses due to beam losses in a novel concept of a proton therapy gantry *J. Phys. Conf. Ser.* **874** 012107
ur Rehman M, Zeidan O A, Willoughby T, Meeks S L, Kelly P and Erhart K 2022 Dosimetric comparison of various spot placement techniques in proton pencil beam scanning *Int. J. Part. Ther.* **9** 54–63
Wan W *et al* 2015 Alternating-gradient canted cosine theta superconducting magnets for future compact proton gantries *Phys. Rev. Spec. Top. Accel Beams* **18** 103501
Wang W *et al* 2023 Improving delivery efficiency using spots and energy layers reduction algorithms based on a large momentum acceptance beamline *Med. Phys.* **50** 5189–200
Wei S, Lin H, Isabelle Choi J, Shi C, Simone C B , 2nd and Kang M 2022 Advanced pencil beam scanning Bragg peak FLASH-RT delivery technique can enhance lung cancer planning treatment outcomes compared to conventional multiple-energy proton PBS techniques *Radiother. Oncol.* **175** 238–47
Wieser H-P *et al* 2017 Development of the open-source dose calculation and optimization toolkit matRad *Med. Phys.* **44** 2556–68
Yan S, Ngoma T A, Ngwa W and Bortfeld T R 2023 Global democratisation of proton radiotherapy *Lancet Oncol.* **24** e245–54
Yan Y L *et al* 2017 Spot-scanning beam delivery with laterally-and longitudinally-mixed spot size pencil beams in heavy ion radiotherapy *Chin. Phys.* C **41** 098201
Yap J, De Franco A and Sheehy S 2021 Future developments in charged particle therapy: improving beam delivery for efficiency and efficacy *Front. Oncol.* **11** 780025
Zhao R, Qin B, Liao Y, Liu X, Chen Q and Han W 2021 Achieving a realistic design for a superconducting gantry with large momentum acceptance for proton therapy *Nucl. Instrum. Methods Phys. Res.* A **1015** 165773